BIOCHEMISTRY
including biophysical chemistry & molecular biology

Article

pubs.acs.org/biochemistry

Enhanced Specificity of the Viral Suppressor of RNA Silencing Protein p19 toward Sequestering of Human MicroRNA-122

Jenny Cheng,[†,⊥] Dana C. Danielson,[†,§,⊥] Neda Nasheri,[†,§] Ragunath Singaravelu,[†,§] and John Paul Pezacki*[,†,‡,§]

[†]Steacie Institute for Molecular Sciences, National Research Council of Canada, 100 Sussex Dr., Ottawa, Canada K1A 0R6

[‡]Department of Chemistry, University of Ottawa, 10 Marie-Curie, Ottawa, Canada K1N 6N5

[§]Department of Biochemistry, Microbiology & Immunology and Ottawa Institute of Systems Biology, University of Ottawa, Health Sciences Campus, 451 Smyth Road, Ottawa, Canada K1H 8M5

Supporting Information

ABSTRACT: Tombusviruses express a 19 kDa protein (p19) that, as a dimeric protein, suppresses the RNAs silencing pathway during infection by binding short-interfering RNA (siRNA) and preventing their association with the RNA-induced silencing complex (RISC). The p19 protein can bind to both endogenous and synthetic siRNAs with a high degree of size selectivity but with little sequence dependence. It also binds to other endogenous small RNAs such as microRNAs (miRNAs) but with lower affinity than to canonical siRNAs. It has become apparent, however, that miRNAs play a large role in gene regulation; their influence extends to expression and processing that affects virtually all eukaryotic processes. In order to develop new tools to study endogenous small RNAs, proteins that suppress specific miRNAs are required. Herein we describe mutational analysis of the p19 binding surface with the aim of creating p19 mutants with increased affinity for miR-122. By site-directed mutagenesis of a single residue, we describe p19 mutants with a nearly 50-fold increased affinity for miR-122 without altering the affinity for siRNA. Upon further mutational analysis of this site, we postulate that the higher affinity relies on hydrogen-bonding interactions but can be sterically hindered by residues with bulky side chains. Finally, we demonstrate the effectiveness of a mutant p19, p19-T111S, at sequestering miR-122 in human hepatoma cell lines, as compared to wild-type p19. Overall, our results suggest that p19 can be engineered to enhance its affinity toward specific small RNA molecules, particularly noncanonical miRNAs that are distinguishable based on locations of base-pair mismatches. The p19-T111S mutant also represents a new tool for the study of the function of miR-122 in post-transcriptional silencing in the human liver.

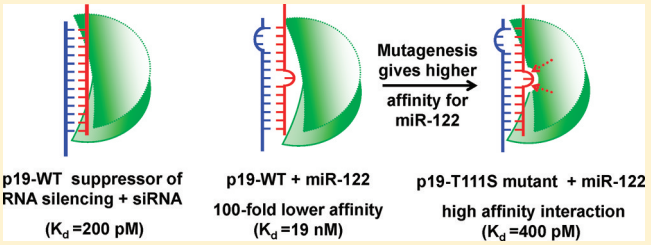

In the past decade, it has become apparent that small, noncoding RNAs are key regulators of gene expression and influence virtually all eukaryotic cellular processes.[1,2] These small RNAs (~20−30 nucleotides in length) inhibit specific gene expression as determined by their nucleotide sequence. Small RNAs have double-stranded RNA (dsRNA) precursors that can be derived transcriptionally or from exogenous sources. The RNA silencing pathway in cells is responsible for excising small dsRNAs of a characteristic length from their precursors, subsequently unwinding the duplex, locating the complementary target RNA sequence, and ultimately inhibiting its expression.[1] The RNA silencing pathway serves a critical role in the cellular innate immune response to dsRNA. Particularly in plants, the pathway serves as an antiviral response by generating small interfering RNAs (siRNAs) which inhibit replication of the viral genome.[2]

Although the RNA silencing response to dsRNA is extremely potent, several RNA viruses have evolved mechanisms of inhibiting the pathway, thereby allowing viral propagation in their host. Tombusviruses, such as Carnation Italian Ringspot Virus (CIRV), are a family of RNA plant viruses that express a 19 kDa protein, p19, which, as a dimer, binds small dsRNAs with nanomolar affinity, thus preventing their incorporation into the RNA-induced silencing complex (RISC).[3,4] The binding is based on hydrogen-bonding and electrostatic interactions between the β-sheet surface of the homodimer and the sugar−phosphate backbone of the siRNA, thereby allowing sequence-independent binding.[5,6] p19 displays specificity based on size of the siRNA, preferentially binding 21-nt siRNAs with a dramatic drop in affinity for longer species. This size selectivity is determined by two pairs of tryptophan residues which provide end-capping interactions that stabilize a 21-nt siRNA in the binding pocket of the dimer.[5−7] Because of its unique binding properties, p19 has been used as an effective suppressor of RNA silencing in a variety of systems, including plants,[8,9] human cells,[9,10] *Caenorhabditis elegans*,[11] and mouse embryonic stem cells.[12] The p19 protein has also been used to profile miRNA levels as part of an enzyme immunoassay[13] and track viral infection

Received: May 28, 2011
Revised: August 4, 2011
Published: August 5, 2011

in plants using a p19-GFP fusion reporter protein.[14] Furthermore, we have engineered higher affinity p19 mutants[15] as well as p19 fluorescent fusion constructs which sense p19 binding to small RNAs based on Förster resonance energy transfer (FRET).[16]

It has also been shown that p19 binds another class of small RNA molecules, microRNAs (miRNAs), with high affinity.[7,8,10] miRNAs are transcribed from noncoding regions of the genome and regulate expression of endogenous genes. Specific miRNA expression profiles correlate with tissue type and phases of development. Disregulation of these profiles is associated with several human pathologies, including cancer.[17] Additionally, viruses modulate host miRNA expression as well as express their own virally encoded miRNAs in order to facilitate their pathogenesis.[18] MicroRNA-122 is a liver specific miRNA[19,20] whose expression has been shown to positively regulate the replication, translation, and virion production of the hepatitis C virus.[21−24] Consequently, means of miR-122 sequestration are presently being investigated as an antiviral strategy.[25]

We hypothesize that p19 can be engineered to have high affinity and specificity for miR-122, which would allow it to be used to sequester miR-122 in biological systems and potentially serve as a novel antiviral tool. We have previously reported that p19 has the ability to bind miR-122 with nanomolar affinity, although with substantially lower affinity than for its canonical 21-nt siRNA ligands.[7] The differences in affinity are likely because, unlike siRNAs, miRNAs are irregularly shaped due to mismatches in their nucleotide sequence, which create bulges in their secondary structure, potentially hindering interactions with p19. In this work, we aim to identify residues in p19 that interact with miR-122 uniquely in order to better understand the interaction and develop p19 mutants with higher affinity for miR-122. We have targeted the residues of the p19 binding site we predict to interact with secondary structure elements of the miR-122 molecule. Through site-directed mutagenesis, we have identified several residues that affect p19's binding affinity for miR-122 and describe two mutants of p19 which display a nearly 50-fold higher affinity for miR-122 compared to wild type. Furthermore, we demonstrate one of the p19 mutant's effectiveness at sequestering miR-122 in human hepatoma cell lines. This work lays the foundation for the use of mutant p19 proteins for the study of miRNAs, providing a protein-based sequestration tool for miRNAs such as miR-122. This technology will help elucidate the role of miRNAs in regulating biological systems such as liver function as well as studying their interactions with other targets such as viral genomes.

EXPERIMENTAL PROCEDURES

DNA Oligonucleotides and Fluorescently Labeled siRNAs. All DNA oligos used in the cloning experiments were purchased from Sigma GenoSys (Oakville, ON) and purified by reverse-phase cartridge purification. All RNAs were synthesized by Dharmacon (Lafayette, CO), purified by polyacrylamide gel electrophoresis (PAGE), and desalted using reverse-phase HPLC. The purity was demonstrated to be >95% according to the manufacturer's specifications. The duplexed siRNAs used in the electrophoretic mobility shift assay have the following sense and antisense sequences, respectively: Cy3-CSK siRNA (21-mer) 5′-Cy3-CUA CCG CAU CAU GUA CCA UdTdT-3′ and 5′-AUG GUA CAU GAU GCG GUA GdTdT-3′; Cy3-GL2 siRNA (28-mer) 5′-Cy3-ACA UCA CGU ACG CGG AAU ACU UCG AAdT dT-3′ and 5′-UUC GAA GUA UUC CGC GUA CGU GAU GUdT dT-3′. The Cy3-labeled miR-122 (Cy3-miR-122) used has the following sense and antisense sequences, respectively: 5′-Cy3-AAA CGC CAU UAU CAC ACU AAA UA-3′ and 5′-UGG AGU GUG ACA AUG GUG UUU GU-3′. Both strands were deprotected, annealed, and precipitated according to the manufacturer's protocols. To ensure that all of the labeled strands were duplexed, we used a slight excess of the unlabeled strand during annealing of Cy3-miR-122 duplex. The 21-nucleotide (nt) Cy3-labeled single-stranded (ss) RNA (Cy3-ssRNA) has the following sequence: 5′-Cy3-CGU ACG CGG AAU ACU UCG AUU-3′.

Cell Culture. Huh7.5 human hepatoma cells were grown in an incubator at 37 °C with 5% CO_2, in cell culture medium, i.e., Dulbecco's Modified Eagle Medium (DMEM) (Gibco-Invitrogen), supplemented with 10% fetal bovine serum (FBS), 100 nM nonessential amino acids (NEAA), 50 U/mL penicillin, and 50 μg/mL streptomycin.

Plasmid Construction and Site-Directed Mutagenesis. Construction of the pTriEx-p19 plasmid encoding the wild-type, codon-optimized Carnation Italian Ringspot virus p19 protein (p19-WT) with a C-terminal octahistidine tag (8xHis-tag) was described previously.[26] Construction of various mutant p19 candidates with enhanced miR-122 affinity was performed using the QuikChange II site-directed mutagenesis kit (Stratagene) according to manufacturer's protocol. The template DNA for the mutagenesis and the complementary primer pairs used for the mutated constructs are described in Table S1 of the Supporting Information. All constructed DNA plasmids were confirmed by DNA sequencing.

Protein Expression and Purification. Bacterial expression of the His-tagged p19-WT and mutant derivatives was carried out as previously described[26] with the following modifications. Briefly, *E. coli* strain BL21 (DE3) cells harboring the p19 constructs were grown at 37 °C until an optical density at 600 nm (OD_{600}) of 0.5−0.6 was achieved. Expression of p19 proteins was induced by IPTG at a final concentration of 1 mM. Cultures were then grown for an additional 3−4 h at 28 °C or until OD_{600} reached ∼1.5. After harvesting, bacterial pellets were resuspended in lysis buffer (50 mM Tris, 300 mM NaCl, 10 mM imidazole, 1 mM dithiothreitol (DTT), 1X Complete EDTA-free Protease Inhibitor Cocktail (Roche), pH 8.0) and lysed by sonication on ice bath. Cell lysate was then centrifuged at 20000*g* for 20 min at 4 °C. The soluble lysate fraction containing the His-tagged p19 proteins was loaded to HisTrap FF Ni^{2+}-affinity column (GE Healthcare, Piscataway, NJ). After protein binding, the resin was washed with 10 column volumes of wash buffer (50 mM Tris, 300 mM NaCl, 50 mM imidazole, pH 8.0). Elution of the His-tagged p19 proteins was carried out using elution buffer (50 mM NaH_2PO_4, 300 mM NaCl, 250 mM imidazole, pH 8.0), and 10 mM of DTT was added immediately to the eluate. The pooled eluates were concentrated to 0.5 mL using the Amicon Ultra 10-kDa MWCO centrifugal filter device (Millipore, Concord, MA). The concentrated samples were then injected into Superdex 200 size exclusion column (GE Healthcare, Piscataway, NJ) at a flow rate of 0.5 mL/min. The p19 proteins eluted as stable dimers and were recalcitrant to denaturation even upon boiling for 15−20 min.[15,26,27] Fractions containing the desired p19 proteins, as determined by SDS−PAGE analyses, were pooled and stored at 4 °C for subsequent assays and analyses. Pooled p19 fractions were

monitored by SDS−PAGE as a single band and estimated to be >95% pure.

Electrophoretic Mobility Shift Assay (EMSA) and Data Analysis. For EMSA binding experiments, samples were prepared by incubating 2 nM Cy3-labeled small RNAs with various concentrations of purified p19 or its mutant derivatives in buffer containing 20 mM Tris, 100 mM NaCl, 1 mM EDTA, 0.02% v/v TritonX-100, 2 mM DTT, pH 7 for 1 h at room temperature. 2 μL of 5X TBE sample buffer (90 mM Tris, 90 mM boric acid, 2 mM EDTA, 15% Ficoll type 400, 0.02% xylene cyanol) was added to 18 μL of binding reaction. 10 μL of each sample was analyzed by electrophoresis at a constant voltage of 100 V for 50 min through a 6% TBE DNA retardation gel in 0.5X TBE running buffer (Novex, Invitrogen). The gels were imaged with Fluorescent Method Bio Image Analyzer III (Hitachi, Japan). Bands corresponding to bound and unbound fluorescently labeled small RNAs were quantified with ImageJ software (National Institutes of Health). The fraction of RNA bound by p19 was determined by taking the value of integrated band intensity corresponding to the p19-bound RNA complex over the sum of integrated band intensities from the complex and unbound RNA. The direct binding experiments were analyzed by plotting the fraction bound values against various concentrations of p19 and fitted according to the following equation (eq 1):

$$\Delta P = \Delta P_{\max} \times \left(\frac{K_d + np + x}{2np} - \sqrt{\left(\frac{K_d + np + x}{2np} \right)^2 - \frac{x}{np}} \right) \quad (1)$$

where ΔP denotes the change in fluorescence intensity, $\Delta P_{\max}$ is the maximal change in fluorescence intensity, K_d is the dissociation constant, n is the number of equivalent sites on the p19 dimer, p is the concentration of labeled small RNA, and x is the concentration of the p19 dimer.

Circular Dichroism (CD) and Thermal Melt Analysis. CD spectra were recorded on ∼5 μM p19-WT, p19-T111S, p19-T111H, p19-T111A, p19-T111Y, or p19-Y73S in 20 mM sodium phosphate pH 7.2, 25 mM NaCl, and 10 mM DTT on a Jasco J-815 CD spectrometer with a 1 mm path length quartz cell at 25 °C. Spectra reflect an average of 8 scans recorded from 250 to 190 nm with a 0.2 nm step resolution, response of 1 s, a speed of 20 nm/min, and a bandwidth of 1 nm. Following CD spectroscopy, the concentration of the samples was determined using the Bio-Rad Protein Assay Kit (Bio-Rad, Hercules, CA) and used to calculate the molar ellipticity per mean residue. CD data were analyzed using the CDPro suite of programs.[28] Thermal denaturation of the p19 proteins was performed using a Jasco thermal control unit (model PTC-423S/15) with a heating rate of 1 °C/min from 25 to 95 °C. At each step, the molar ellipticity at 222 nm was recorded.

Transient Expression of His-Tagged p19-WT and p19-T111S in Huh7.5 Cells. For transient expression of p19-WT and p19-T111S, Huh7.5 cells were seeded at 5.0×10^5 cells per 60 mm dish culture media. Cells were transfected once they reached 70% confluency (usually around 24 h postseeding). Prior to transfection, cells were washed once with phosphate-buffered saline (PBS; 137 mM NaCl, 2.7 mM, KCl, 10.1 mM Na_2HPO_4, 1.8 mM KH_2PO_4, pH 7.4) and then with transfection media, i.e., OptiMEM (Invitrogen), while preparing transfection complexes. Transfection complexes were prepared by mixing 7 μg of pTriEx-p19 or pTriEx-p19-T111S DNA plasmid or no DNA (mock) with 14 μL of Lipofectamine 2000 (Invitrogen) in 2.5 mL of transfection media and incubating at room temperature for 20 min. Each transfection complex mixture was then added to the cells and incubated for 4 h at 37 °C. After 4 h, one equivalent volume of recovery media, i.e., antibiotic-free DMEM containing 20% (v/v) FBS and 100 nM minimal nonessential amino acids, was added. Transfected cells were then incubated at 37 °C and 5% CO_2 for 24 h.

Western Blot Analysis of Transient Expression of His-Tagged p19-WT and p19-T111S in Huh7.5 Cells. Cells were washed twice with PBS and lysed with a lysis buffer consisting of 50 mM Tris-HCl (pH 6.8), 2% SDS, and 10% glycerol 24 h post-transfection. A protease inhibitor cocktail mix (Roche Diagnostics, Penzberg, Germany) was added to each extract. The protein concentration of the whole cell lysate was quantified by using the Bio-Rad DC Protein Assay according to the manufacturer's protocol. Prior to loading, a final concentration of 100 mM DTT and 0.1% v/v bromophenol blue was added to each sample. A total of 50 μg protein/well was loaded onto a 12% SDS−PAGE gel. The resolved proteins were transferred to a Hybond-P (Amersham Biosciences, Piscataway, NJ) poly(vinylidene difluoride) membrane. The membrane was probed against a horseradish peroxidase (HRP)-conjugated monoclonal anti-His-tag antibody (1:5000 dilution; R & D Systems, Inc., Minneapolis, MN). As a loading control, membranes were stripped and reprobed using a mouse anti-PTP-1D 1° antibody (1:2500 dilution; Sigma, Saint Louis, MO) followed by a 2° HRP-conjugated goat anti-mouse IgG antibody (1:10,000 dilution; Jackson ImmunoResearch Laboratories, Inc., Westgrove, PA). The blot was developed using ECL Plus Western Blotting Detection Reagents (GE Healthcare, Baie d'urfe, QC) according to the manufacturer's protocol. The band intensities were measured by densitometry using ImageJ software (National Institutes of Health).

Quantification of miRNA Bound by His-Tagged p19. Twenty-four hours post-transfection, cells were trypsinized and washed twice with PBS by centrifugation at 1000 rpm, 5 min at room temperature. Cells were then lysed by resuspending the cell pellet with lysis buffer (pH 8) containing 150 mM KCl, 50 mM HEPES, 0.5% v/v NP-40, 0.5 mM DTT, 1X Complete EDTA-Free Protease Inhibitor Cocktail (Roche), and 100 U/mL RNaseOUT (Invitrogen) and incubation at 4 °C with rotation for 10 min. The lysate was passed through a 0.2 μm filter unit to remove cell debris. Filtered lysate was loaded onto a 1 mL HisTrap FF column (GE Healthcare, Piscataway, NJ) that was prepared RNase-free by washing with the following RNase-free solution: 10 column volume (CV) 0.1 M NaOH, 0.05 NaCl, 10 CV water, and then equilibrated with 10 CV lysis buffer without DTT, to capture any His-tagged p19 that was transiently expressed in the cell. The His-tagged p19 proteins bound to the column were eluted with buffer containing 50 mM Tris pH 8, 100 mM NaCl, 50 mM EDTA. The elution fraction was collected for subsequent qPCR analysis.

Total RNA was extracted from the eluate using miRVana miRNA Isolation Kit (Ambion) according to the manufacturer's protocol. 10 ng of the total RNA was reverse transcribed

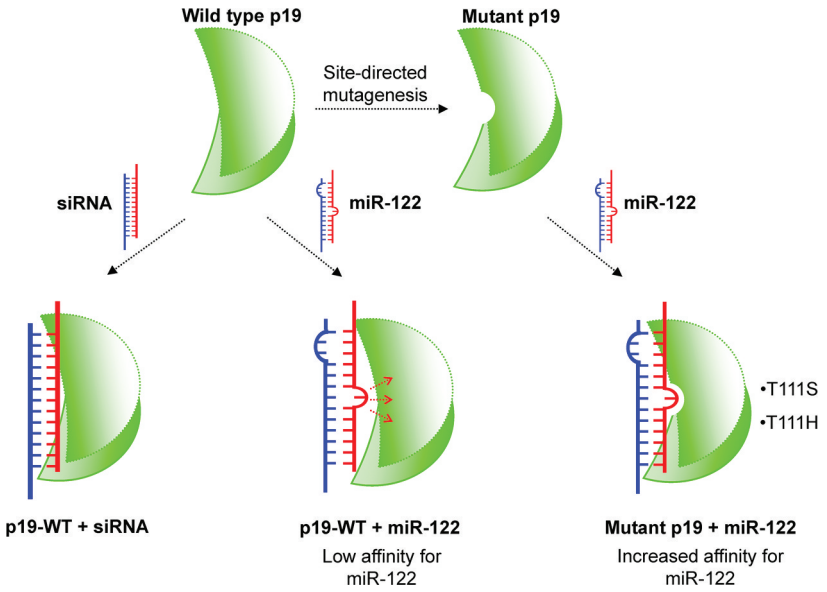

Figure 1. Depiction of the site-directed mutagenesis strategy for identifying p19 mutants with enhanced affinity for miR-122. p19 residues predicted to be interacting with the bulges in the secondary structure of miR-122 were mutated in order to potentially create new, high affinity binding interactions. Substitution of Thr111 with a serine or histidine residue resulted in high affinity binding which enhanced binding to miR-122 without altering its affinity for siRNA.

using the TaqMan MicroRNA Reverse Transcription Kit (Applied Biosystems, Foster City, CA) in combination with the RT stem-loop primers against U6 RNA (endogenous control) (P/N:4427975, Applied Biosystems) and miR-122 (P/N:4427975, Applied Biosystems) according to manufacturer's instructions. miRNA levels were analyzed using the Taqman real-time (qRT-PCR) method.[29] Each PCR sample included 1X Universal Taqman PCR Mastermix (Applied Biosystems), 0.2 mM TaqMan probes against either U6 RNA or miR-122 (Applied Biosystems), 1.5 mM forward primer, and the universal reverse primer. Relative miRNA abundance was calculated using the comparative Ct method.[30] The data represent the average of three independent experiments each performed in triplicates.

RESULTS AND DISCUSSION

Strategy for Mutational Analysis of p19 Binding with miR-122. Previously, we have demonstrated that the p19 protein is able to bind to an irregularly structured miRNA, miR-122, with nanomolar affinity.[7] It was proposed that p19's capability to bind miR-122 with nanomolar affinity is likely due to retention of key interactions observed between p19 and siRNA. Although miR-122 is 23-nt in length, the base-pairing mismatches in the miRNA may slightly compress the length of the molecule, potentially allowing the duplex region to adopt a length closer to the standard 19-base pair (bp) region in an A-form dsRNA duplex observed in a 21-nt siRNA molecule.[6] This compression would facilitate miR-122 to fit between the two end-capping helices of the p19 dimer, thereby retaining the interactions that give p19 its size selective affinity for 21-nt siRNAs. In this case, it is likely that the miRNA docks onto the p19 protein in similar fashion to siRNA but with 2 possible docking orientations due to the presence of asymmetric bulges in the miR-122 molecule. Notably, p19 displays ~100-fold reduction in affinity for miR-122 compared to 21-nt siRNA, likely due to perturbations to the known p19-siRNA interactions as a result of the structural irregularities arising from the base pair mismatches in the miR-122 duplex.[7] Therefore, we performed mutational analysis of residues predicted to interact with the structural irregularities of miR-122, with the aim of creating a more accommodating binding site which would give rise to higher affinity binding. Our initial strategy was to create "pockets" on the binding surface of p19 to accommodate the bulges of miR-122 by mutating residues on p19's binding surface to residues with smaller side chains. This approach is conceptually similar to the bump-hole approach developed by Shokat and coworkers that have been very successfully applied to the study of kinases.[31−33]

The first step in the strategy involved estimating the location of the bulges relative to the residues of the p19 binding site. In order to predict the position of miR-122's bulges, we used the canonical siRNA as a model to represent their locations relative to p19's small RNA binding surface according to the crystal structure.[5] In our previous publication, we had approximated the position of the nucleotide bases of the "compressed" miR-122 molecule in both docking orientations relative to the bases of the siRNA.[7] The first bulge is due to a 1-bp mismatch in the middle of the miR-122 sequence, which we estimate to be aligned with the siRNA base pair C10-G10′, in both possible docking orientations (Figure 2). Another 2-bp mismatch exists at the side of the miR-122 molecule, which we estimate to be aligned with the siRNA base pairs G2-C18′ and U3-A17′ in docking orientation 1 and with base pairs A17-U3′ and C18-G2′ of the siRNA in docking orientation 2 (Figure 2). These bases of the siRNA were then used to estimate which residues of the p19 binding surface are in proximity to the bulge in the miR-122 molecule.

The small RNA binding surface of p19 consists of an 8-stranded β-sheet as a result of p19 dimerization.[5] Using a molecular viewer program, we identified residues on the β-sheet with side chains facing the interface which displayed no direct interaction with siRNA according to the crystal structure.[5] Substitution of these residues minimizes the chance

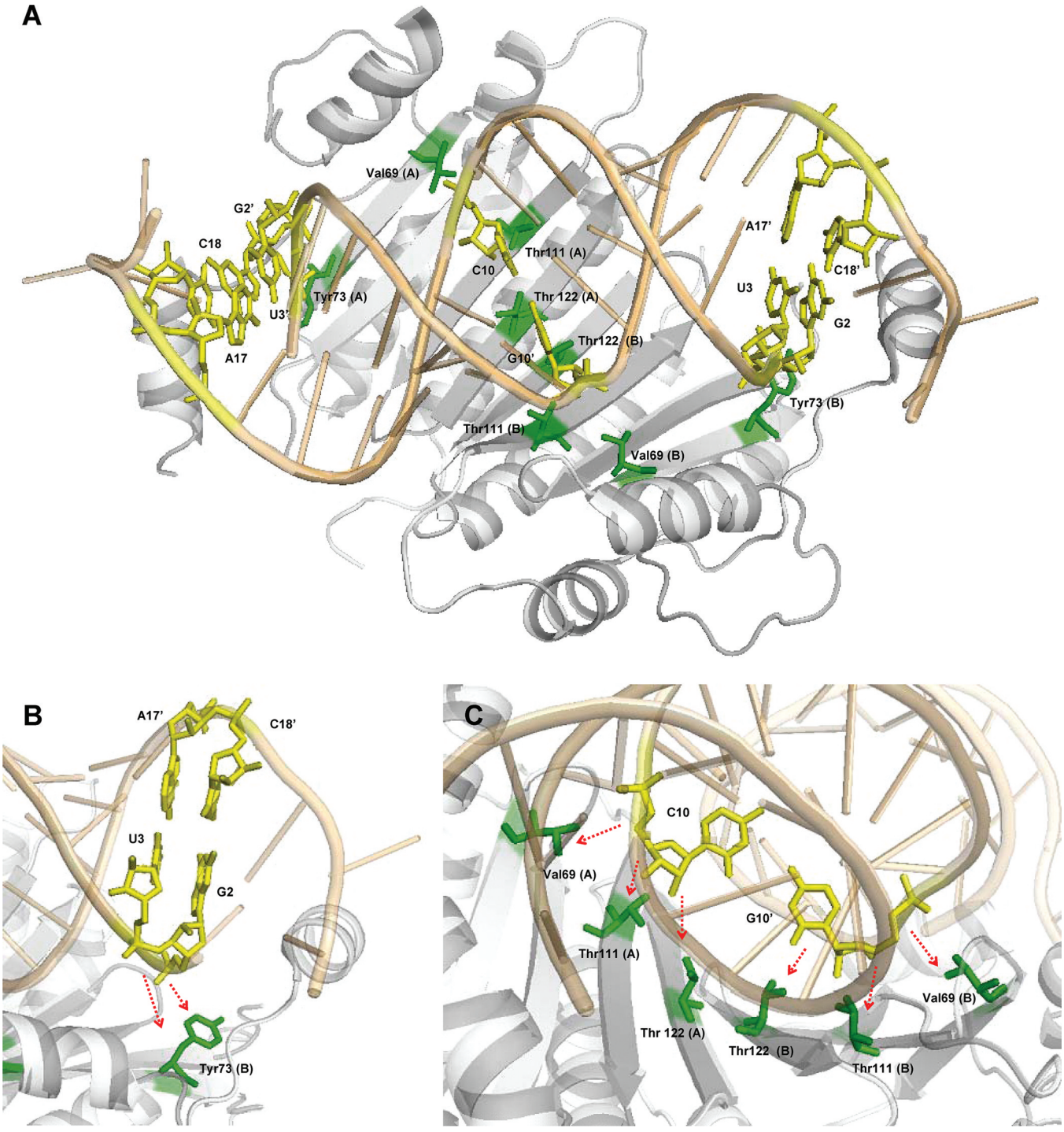

Figure 2. Mutagenesis strategy for altering the p19 binding site based on structural predictions. (A) A ribbon diagram of CIRV p19 crystal structure in complex with siRNA[5] (PDB code: 1RPU). Nucleotide bases of the siRNA molecule that are hypothesized to be in similar location as the bulges in the miR-122 molecule (from both docking orientations) are highlighted in yellow. The residues of the p19 binding surface which are predicted to be in close proximity to the bulges in miR-122 are highlighted in green. These residues (Val69, Tyr73, Thr111, and Thr122) are located on the RNA-binding surface of p19 but do not display any direct interaction with the siRNA. The p19 amino acid residues from each monomer subunit are distinguished by designating them A and B. The siRNA bases from each strand are distinguished by number priming. (B) Base-pairing mismatch of the side bulge in miR-122 represented by base pairs G2′-C18 and U3′-A17 in the siRNA molecule. The mismatch may cause both G2′ and U3″ to push back in the direction as indicated by the red arrows against the residue in green. (C) Base-pairing mismatch of the middle bulge in miR-122 as represented by base pair C10-G10′ in the siRNA molecule. The mismatch may cause both C10 and G10′ to push back in the direction as indicated by the red arrows against the p19 residues in green.

of disrupting key interactions between p19 and the rest of the miR-122 molecule since the majority of interactions that p19 has with siRNA are thought to be retained with miR-122.[7] Out of these candidates, we identified residues that are also proximal to the hypothesized location of the miR-122 bulges (see Figure 2A). This approach resulted in 4 potential sites for

dx.doi.org/10.1021/bi2008273 | *Biochemistry* 2011, 50, 7745–7755

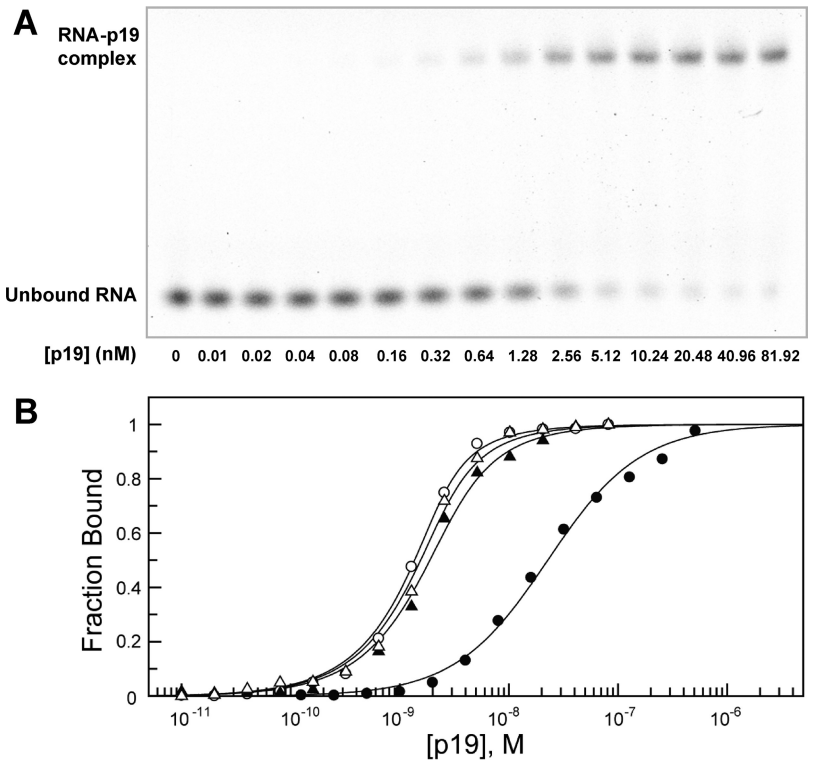

Figure 3. Electrophoretic mobility shift assay of p19-small RNA interactions. (A) A representative gel obtained from an electrophoretic mobility shift assay performed with 2 nM Cy3-labeled CSK-siRNA (21-mer) and various concentrations of p19 protein. (B) Representative analysis of direct binding between p19-WT with 21-mer CSK-siRNA (open circle), p19-WT with miR-122 (closed circle), p19-T111S with CSK-siRNA (open triangle), and p19-T111S with miR-122 (closed triangle). The fraction of RNA bound by p19 (the band intensity corresponding to the band shift of p19-RNA complex formation over the sum of band intensities from the complex and unbound RNA) is plotted against various concentrations of p19.

mutagenesis experiments at residues Val69, Tyr73, Thr111, and Thr122 of p19.

The side bulge of the miR-122 molecule caused by a 2-nt mismatch is parallel to G2 and U3 in the siRNA molecule in docking orientation 1 or G2′ and U3′ in docking orientation 2 (Figure 2). The Tyr73 residues in both p19 monomers are predicted to be in proximity to the side bulge of the miR-122 molecule in each of the two possible docking orientations, respectively, due to the asymmetry in the miR-122 molecule (Figure 2A). Assuming the side bulge of miR-122 pushes back against the p19 surface close to Tyr73 (Figure 2B), we hypothesized that mutating this tyrosine to a smaller residue could reduce any potentially unfavorable steric interactions and allow for a better fit for the miR-122 into the p19 dimer. Therefore, substituting the Tyr73 residues in both p19 monomers to a serine residue would eliminate the bulky benzene ring while preserving the hydroxyl group for any potential new interactions, such as hydrogen bonding with the phosphate backbone of the miR-122 molecule. Residues Val69, Thr111, and Thr122 in both p19 monomers are predicted to be in proximity to the middle bulge of the miR-122 molecule in both docking orientations (Figure 2A). The middle bulge, as a result of 1-nt mismatch, is represented as C10 and G10′ in the siRNA molecule (Figure 2A). Assuming the mismatch causes C10 and G10′ to push away from each other, they may possibly be forced against Val69, Thr111, and/or Thr122 in both p19 monomers (Figure 2C). Hence, mutating Val69, Thr111, and Thr122 to residues with smaller side chains may also aid in accommodating the middle bulge. For Thr111 and Thr122, substitution to a serine residue will reduce the size of the side chain by a methyl group while retaining the hydroxyl group for any potential new interactions with the miR-122 phosphate backbone. For Val69, we decided to substitute to an alanine instead of a glycine residue since glycine is thought to be destabilizing for β-sheet structure[34−37] which could have been detrimental to the global structure and stability of p19.

Therefore, the first set of 4 His-tagged p19 mutants included p19-V69A, p19-Y73S, p19-T111S, and p19-T122S, as suggested above, were created by site-directed mutagenesis. The mutant constructs were overexpressed in *E. coli*, purified by Ni^{2+}-affinity chromatography and then with size exclusion chromatography to >95% purity as determined by SDS−PAGE analysis (Figure S1 of Supporting Information). All p19 mutants were shown to have similar size exclusion elution profiles as wild-type p19 (data not shown), suggesting that the introduced mutation did not disrupt p19 dimerization, which is essential for its binding to small RNAs.[5,6] The purified samples were subjected to subsequent analyses.

Enhanced Affinity of p19-T111S for miR-122 *in vitro*. To investigate whether the p19 mutants have enhanced affinity for miR-122 and how their binding behaviors to other small RNAs compare to wild-type p19, electrophoretic mobility shift assays (EMSA) were performed. This technique is commonly used to assess protein−nucleic acid interactions, including the interactions between p19 or p19-GST fusion protein with small RNAs.[4−7,14,38] In our previous study, we analyzed the binding affinity and specificity of p19 with various small RNAs using fluorescence-based EMSAs, and the results were consistent with

dx.doi.org/10.1021/bi2008273 | *Biochemistry* 2011, 50, 7745−7755

values measured by fluorescence polarization, a method that gives the true equilibrium of the molecular interactions.[39,40]

The EMSA experiments were performed by complexing Cy3-labeled RNA with various concentrations of p19 in solution. Figure 3A illustrates a representative EMSA experiment showing the interaction between the p19 and the Cy3-labeled CSK siRNA (21-mer). There is a gradual increase in the fluorescence intensity of the slower migrating bands with an increase in p19 concentration, corresponding to an increase in the labeled small RNA population in complex with p19. In contrast, there was a gradual decrease in intensity of the faster migrating bands corresponding to unbound labeled miRNA. The band intensities corresponding to the p19-small RNA complex and the unbound RNA were measured by densitometry and plotted as a function of p19 concentration. The curves of the direct binding experiment also show a dose–response relationship between the small RNAs and p19 (Figure 3B).

Out of the initial four p19 mutants generated, p19-T111S was the sole mutant to display enhanced affinity for miR-122 relative to wild type. Mutants p19-V69A and p19-T122S both show significantly reduced ability to bind miR-122; therefore, we did not pursue those constructs for further analysis (Table S2 of Supporting Information). In the more extreme case, p19-Y73S shows no observable binding (Table S2 of Supporting Information). The dissociation constant of p19-T111S with Cy3-miR-122 obtained by EMSA (0.4 ± 0.1 nM) was found to be almost 50-fold enhancement compared to wild type (19 ± 4 nM) (Table 1). Notably, T111S displayed minimal difference in binding affinity for the canonical ligand, 21-nt siRNA (0.27 ± 0.06 nM), compared to wild-type p19 (0.21 ± 0.05 nM) (Table 1).

Table 1. Dissociation Constants (K_d) of p19-WT and T111 Mutants with Small RNAs

	K_d (nM)	
	Cy3-miR-122	Cy3-CSK siRNA (21-mer)
p19-WT	19 ± 4	0.21 ± 0.05
p19-T111S	0.4 ± 0.1	0.27 ± 0.06
p19-T111H	0.4 ± 0.1	0.21 ± 0.02
p19-T111Y	6 ± 1	0.38 ± 0.08
p19-T111A	>100[a]	0.24 ± 0.06

[a]Saturation of binding was not achieved at concentration up to 1 μM of the p19 protein.

To ensure that the p19-T111S retained the selective binding properties of wild-type p19, we analyzed its binding to a longer siRNA (28-mer) and a 21-nt single-stranded (ss) RNA by EMSA. We were unable to reach saturation using the 28-mer siRNA due to solubility limitation of the p19 protein, but the dissociation constant was estimated to be in the 10 μM range (Table S2 of Supporting Information). Similarly, p19-T111S displayed no binding for the 21-nt ssRNA (Table S2 of Supporting Information) as no slower migrating band corresponding to p19-small RNA complex was observed. The results demonstrate that, along with the enhanced affinity to miR-122, the p19-T111S mutant retains the size selectivity and specificity to 21-nt siRNA duplex which is consistent with the known binding behavior of wild-type p19 from previous studies.[5,7,15]

Mutational Analyses of the Thr111 p19 Residue. To further investigate the high-affinity binding resulting from mutating T111S, we created three other mutants at this position: T111H, T111A, and T111Y. As mentioned, our initial strategy was based on creating a "pocket" in the p19 binding site to accommodate the bulges in miR-122. We chose to expand the mutational analysis at this site in order to delineate whether the high affinity binding of p19-T111S was due to a decrease in size of the side chain and/or the formation of new hydrogen-bonding interactions. By comparing the binding affinities of all the T111 mutants for miR-122 using EMSA, we have deduced that retaining the hydrogen-bonding capacity of the residue at the 111 position is more critical for high-affinity binding of miR-122 than simply creating a "pocket" with a smaller residue. The T111H mutant, which possesses a slightly bulkier side chain but retains hydrogen-bonding capacity, displays the same high affinity for miR-122 (0.4 ± 0.1 nM) as T111S, whereas T111A, with a smaller side chain but no hydrogen bonding capacity, displays a dramatically reduced affinity for miR-122 (>100 nM) compared to wild-type p19. The T111Y mutant, with a bulky, aromatic side chain but also hydrogen-bonding capacity, did not bind as well as the T111S mutant, although still exhibits a modest (~3-fold) increase in affinity for miR-122 than wild-type p19. Overall, the data suggest that the increase in affinity of the p19-T111S and p19-T111H mutants for miR-122 rely on forming new hydrogen-bonding interactions which are not available with threonine. The differences between the interactions provided by threonine and the mutated residues suggest that the new, high affinity interactions between residue 111 and miR-122

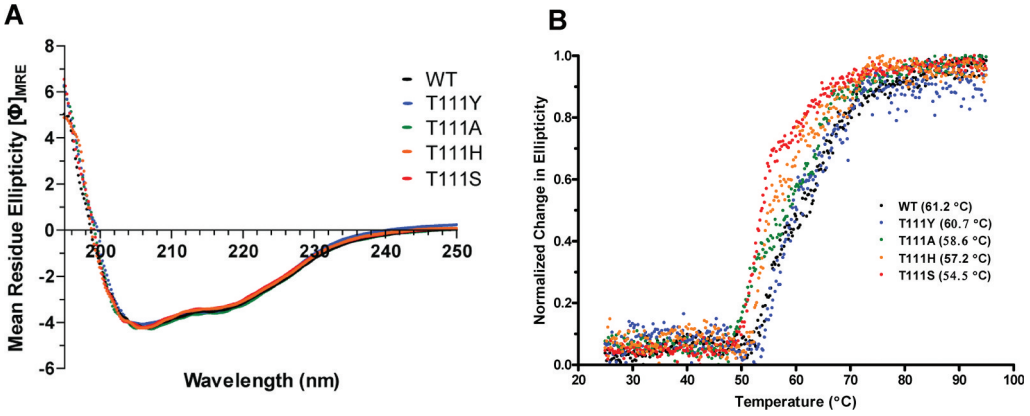

Figure 4. Circular dichroism of p19-WT and p19-T111S: (A) far-UV spectra and (B) thermal denaturation profiles monitored at 222 nm.

dx.doi.org/10.1021/bi2008273 | Biochemistry 2011, 50, 7745–7755

require specific orientations of the side chain. Additionally, these new interactions appear somewhat susceptible to steric interference, where bulkier side chains capable of hydrogen bonding do not provide high-affinity interactions with miR-122.

Notably, the mutations at the T111 residue do not result in significant changes to the affinity of p19 for its canonical ligand, 21-nt siRNA (Table 1). This is consistent with the X-ray crystal structure that no observable interaction is formed between Thr111 and siRNA.[5] Our data suggests that, as hypothesized, p19 binding miR-122 retains the majority of the interactions which allow siRNA binding. Importantly, the data suggest that there are unique interactions between p19 and miR-122 which are not involved in p19 binding siRNA. This observation substantiates the possibility of engineering p19 mutants with high affinity and selectivity for miR-122.

Structural and Thermal Analysis of p19-T111 Mutants with Circular Dichroism. In order to determine whether there were any large structural changes associated with the p19-T111 mutants, circular dichroism (CD) spectra were acquired and compared to wild-type p19. As shown in Figure 4A, the far-UV CD spectra of wild-type p19 and all of the p19 T111 mutants overlap well with each other, and all possessed minima at 208 and 222 nm, suggesting significant α-helical content. This was confirmed by secondary structure deconvolution using the suite of programs provided by CDPro where wild-type p19 displays an average of ~24% α-helical and ~25% β-sheet content, and the mutants display ~23−25% α-helical content and ~25% β-sheet content, except for T111Y, which displays ~27% β-sheet content. The similarity in CD spectra indicates that the secondary structure of wild-type p19 and the p19-T111 mutants are very similar and that the mutation did not introduce significant changes to the global structure of the protein.

Thermal denaturation analysis was also performed on the p19-T111 mutants and compared to that of wild-type p19 by monitoring ellipticity at 222 nm in order to investigate whether any structural changes could be associated with differing affinities of the p19-T111 mutants for miR-122 versus wild-type p19 (Figure 4B). All of the p19-T111 mutants and wild-type p19 showed a significant loss of CD signal intensity over a narrow range of temperatures, with ellipticity values being close to zero at 90 °C. For wild-type p19, the thermal unfolding transition temperature or melting temperature (T_m) is ~61 °C. All of the p19-T111 mutants show a slightly decreased T_m value. The two mutants with increased affinity for miR-122, T111S, and T111H both show the largest decrease in T_m, at ~55 and ~57 °C, respectively. The difference in the denaturation temperatures indicates that the p19-T111 mutants are less thermally stable than the wild-type p19, although the extent of the change does not reflect any decrease in overall viability of the mutants, as can be seen from their binding affinities and size exclusion profiles. The thermostability of proteins has been inversely correlated with protein flexibility.[41,42] The reduced thermostability and thus increased structural flexibility of p19-T111S and p19-T111H may potentially contribute to the enhanced affinity for miR-122. One of our previous rationale for p19's ability to bind miR-122 at nanomolar affinity maybe linked to its inherent flexibility.[7] Conformational flexibility is thought to be important and widely recognized in protein−nucleic acid interactions.[43−45] Specifically in protein−RNA complexes, this is seen in the binding of Ro protein to it is RNA target.[45] In addition, the flexibility in the hinge region of the Dicer enzyme is crucial for its dsRNA binding and processing.[44] Similarly, the increased flexibility of the p19-T111S protein may help ease the fit of the bulky secondary structures inherent in the miR-122 molecule and further enhance the association of the p19-miR-122 complex.

p19-Y73S Mutant Incapable of Binding Small RNA. The p19-Y73S mutant showed no observable binding to siRNA or miR-122. In order to understand why this mutant is incapable of binding, we acquired CD spectra to look for alterations in protein structure. In comparing the CD spectra of p19-Y73S and wild-type p19, we observe a clear difference in the spectra below 210 nm (Figure S2A of Supporting Information). This suggests that the Y73S mutation induces a conformational change in p19. Interestingly, the thermal denaturation analysis of p19-Y73S shows that this mutant has slightly higher thermostability than wild-type p19 (Figure S2B of Supporting Information). It is possible these data reflect that p19-Y73S has adopted a more rigid conformation which is not conducive to ligand binding. From the crystal structure data, it can be seen that there are several basic residues in this region of the C-terminus (R72, R75, R85), which do not contact the siRNA directly but rather form salt bridges to residues on the N-terminus (Glu17, Glu35, Glu41).[5] These salt bridges have been hypothesized to be important for positioning the α-helix of the N-terminus which carries the end-capping tryptophan residues.[5] Previous studies examining the role of p19 in viral infection, symptom induction, and spread in host plants have created mutants of Tomato Bushy Stunt virus (TBSV) p19, where several of the basic residues from this C-terminal region were mutated to glycine (p19-R72G, p19-RR75-78GG), which resulted in p19 losing all of its *in vivo* functionality as a viral suppressor of RNA silencing.[46,47] The R72G mutation, however, likely resulted in buried charged residues which could have altered the global structure of the protein.[5] Further functional studies have used the p19-RR75-78GG mutant to demonstrate the link between siRNA binding and the *in vivo* functionality and symptom induction by p19, since it was demonstrated that p19-RR75-78GG forms dimers that are incapable of capturing siRNA *in vivo*.[27,48] Another residue near to Y73, K71, forms salt bridges with the siRNA sugar phosphate backbone.[5] The null mutant, p19-Y73S, is interesting because, from the crystal structure data, the Y73 residue does not appear to be directly involved in siRNA binding or stabilizing the end-capping helices. Thus, it is possible that either the mutation p19-Y73S alters the salt bridge interactions between nearby residues which have been shown to be crucial for siRNA binding *in vivo* or the Y73 residue is directly responsible for currently unknown interactions critical for binding siRNA. It is possible that the p19-Y73S mutant may be a more appropriate null p19 mutant with potentially less conformational changes that may be associated with the rather drastic mutations of p19-RR75-78GG or p19-R72G. Further mutational analysis of this residue and structural studies are currently being pursued in our laboratory.

Enhanced Affinity of p19-T111S for miR-122 *in situ*. To demonstrate that p19-T111S can also bind miR-122 with higher affinity than p19-WT in a cellular environment, we have established a method to quantify the relative level of miR-122 captured by p19-T111S compared to p19-WT in Huh7.5 cells, a hepatoma cell line that expresses high levels of miR-122[49] as summarized in the schematic diagram in Figure 5. Briefly, Huh7.5 cells transiently expressing His-tagged p19-WT or

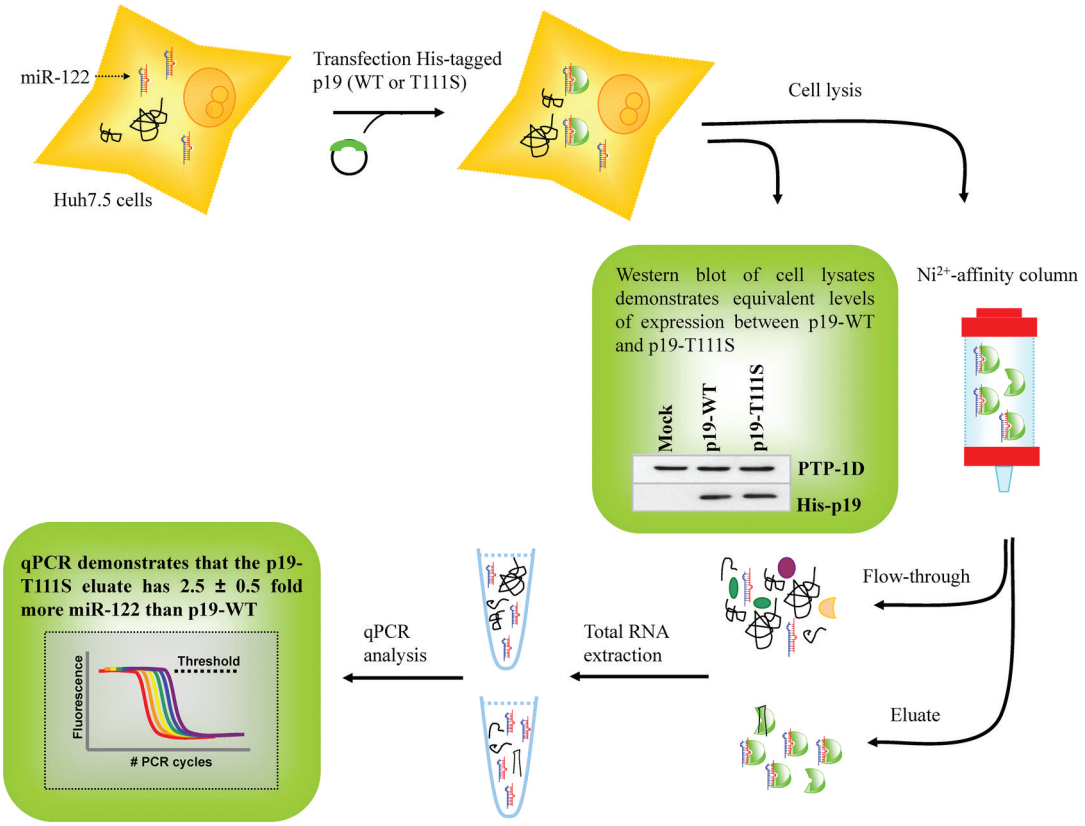

Figure 5. Schematic of the *in situ* miR-122 capture experiment. Huh7.5 cells are transiently transfected with either wild-type p19 or the T111S mutant. After 24 h, cells are lysed and p19 expression is analyzed by Western blot. Cells expressing wild-type p19 and p19-T111S show very similar expression levels, indicated by the relative (%) density of the p19 band to the PTP-1D loading control. The His-tagged p19 proteins in the lysate are then captured on a Ni^{2+}-affinity column. The flow-through fraction and eluate from the column are collected and subject to total RNA extraction. The miR-122 content of the samples is then quantified via qPCR. The high-affinity p19-T111S mutant captured (2.5 ± 0.5)-fold more miR-122 than wild-type p19.

p19-T111S proteins are harvested and lysed. The His-tagged p19 proteins in the lysate are then captured on a Ni^{2+}-affinity column, with the flow-through and the eluate collected for subsequent qPCR analysis. The RNA extracted from the eluate fraction, containing p19 proteins eluted from the column, represents the RNA which was bound to p19. After total RNA extractions, the amount of miR-122 in these fractions was quantified by qPCR using probes against the sequence of miR-122 and subsequently normalized to the expression levels of a reference gene, RNU6B (Figure 5). The result showed that there is a (2.5 ± 0.5)-fold enrichment of miR-122 in the eluate fraction from cells expressing p19-T111S compared to wild type. The flow-through fraction also displayed the expected trend, with more miR-122 present in the p19-WT flow through than the p19-T111S flow through. This *in situ* miRNA sequestration assay suggests that there is a ~2.5-fold enhancement in the sequestration of miR-122 by p19-T111S relative to the wild-type protein in Huh7.5 cells.

■ CONCLUSION

In this work, we describe our mutational analysis of the p19 protein in binding a noncanonical ligand, miR-122, with the aim of creating high-affinity mutants. In our previous studies, we determined p19 as capable of binding this noncanonical ligand, but with lower affinity than for its canonical 21-nt siRNA ligand. By mutating the residues which we have predicted to be interacting with the bulges in the secondary structure of miR-122, we have created two mutants capable of binding miR-122 with nearly ~50-fold higher affinity than wild-type p19. This work shows that it is possible to engineer RNA binding proteins such as p19 for accommodating secondary structure of noncanonical ligands. The higher affinity appears to be due to new interactions which rely on hydrogen bonding but can be sterically hindered by bulky residues. Furthermore, the new interactions created through mutagenesis which affect binding affinity are unique to miR-122 and do not affect the affinity of p19 for siRNA. This observation corroborates our hypothesis that the binding surface of p19 interacts differently with miRNAs than siRNAs, thereby allowing the possibility that p19 may be engineered to bind miR-122 with high affinity and specificity. Our aim to alter p19 to preferentially bind specific small RNAs is motivated by possible applications in interrogating the role of specific small RNAs in infectious model systems. Our focus was to identify mutants of p19 with a higher affinity for miR-122, for use in human cells with potential application in inhibiting hepatitis C viral replication. Theoretically, our approach described here could be used to identify mutants with high affinity for other small RNAs in order to understand their roles in other diseases, infections, and cellular development.

dx.doi.org/10.1021/bi2008273 | *Biochemistry* 2011, 50, 7745–7755

■ ASSOCIATED CONTENT

Supporting Information

Table SI (list of p19 mutants and mutagenic primers used in site directed mutagenesis), Table SII (dissociation constants of p19 wild type and mutants with small RNAs), Figure SI (SDS-PAGE analysis of p19 wild type and mutants), Figure SII (circular dichroism of p19 wild type and mutants). This material is available free of charge via the Internet at http://pubs.acs.org.

■ AUTHOR INFORMATION

Corresponding Author

*E-mail: John.Pezacki@nrc-cnrc.gc.ca. Tel: 613-993-7253. Fax: 613-941-8447.

Author Contributions

⊥These authors contributed equally to this work.

■ ACKNOWLEDGMENTS

J.P.P. thanks the Genomics and Health Initiative of the National Research Council of Canada and the Natural Sciences and Engineering Research Council of Canada (NSERC) for funding this work. D.C.D. thanks NSERC for funding in the form of an NSERC CGS-M scholarship. R.S. thanks NSERC for a Vanier Graduate Scholarship and the CIHR National Canadian Research Training Program in Hepatitis C for additional support. We thank Dr. Roger MacKenzie from the Institute of Biological Sciences at the National Research Council Canada for the use of the FPLC system for the protein purification and CD instrument for structural analysis.

■ ABBREVIATIONS

CD, circular dichroism; CIRV, Carnation Italian Ringspot virus; CSK, carboxyl-terminal Src kinase; dsRNA, double-stranded RNA; EMSA, electrophoretic mobility shift assay; HCV, hepatitis C virus; His_8-tag, octahistidine tag; miRNA, microRNA; qPCR, quantitative polymerase chain reaction; RISC, RNA-induced silencing complex; siRNA, short-interfering RNA; TBSV, Tomato Bushy Stunt virus.

■ REFERENCES

(1) Carthew, R. W., and Sontheimer, E. J. (2009) Origins and Mechanisms of miRNAs and siRNAs. *Cell 136*, 642−655.

(2) Hannon, G. J. (2002) RNA interference. *Nature 418*, 244−251.

(3) Russo, M., Burgyan, J., and Martelli, G. P. (1994) Molecular-Biology of Tombusviridae. *Adv.Virus Res. 44*, 381−428.

(4) Silhavy, D., Molnar, A., Lucioli, A., Szittya, G., Hornyik, C., Tavazza, M., and Burgyan, J. (2002) A viral protein suppresses RNA silencing and binds silencing-generated, 21- to 25-nucleotide double-stranded RNAs. *EMBO J. 21*, 3070−3080.

(5) Vargason, J. M., Szittya, G., Burgyan, J., and Hall, T. M. T. (2003) Size selective recognition of siRNA by an RNA silencing suppressor. *Cell 115*, 799−811.

(6) Ye, K. Q., Malinina, L., and Patel, D. J. (2003) Recognition of small interfering RNA by a viral suppressor of RNA silencing. *Nature 426*, 874−878.

(7) Cheng, J., Sagan, S. M., Jakubek, Z. J., and Pezacki, J. P. (2008) Studies of the interaction of the viral suppressor of RNA silencing protein p19 with small RNAs using fluorescence polarization. *Biochemistry 47*, 8130−8138.

(8) Chapman, E. J., Prokhnevsky, A. I., Gopinath, K., Dolja, V. V., and Carrington, J. C. (2004) Viral RNA silencing suppressors inhibit the microRNA pathway at an intermediate step. *Genes Dev. 18*, 1179−1186.

(9) Dunoyer, P., Lecellier, C. H., Parizotto, E. A., Himber, C., and Voinnet, O. (2004) Probing the microRNA and small interfering RNA pathways with virus-encoded suppressors of RNA silencing. *Plant Cell 16*, 1235−1250.

(10) Lecellier, C. H., Dunoyer, P., Arar, K., Lehmann-Che, J., Eyquem, S., Himber, C., Saib, A., and Voinnet, O. (2005) A cellular microRNA mediates antiviral defense in human cells. *Science 308*, 557−560.

(11) Lu, R., Maduro, M., Li, F., Li, H. W., Broitman-Maduro, G., Li, W. X., and Ding, S. W. (2005) Animal virus replication and RNAi-mediated antiviral silencing in Caenorhabditis elegans. *Nature 436*, 1040−1043.

(12) Calabrese, J. M., and Sharp, P. A. (2006) Characterization of the short RNAs bound by the P19 suppressor of RNA silencing in mouse embryonic stem cells. *RNA 12*, 2092−2102.

(13) Nasheri, N., Cheng, J., Singaravelu, R., Wu, P., McDermott, M. T., and Pezacki, J. P. (2011) An enzyme-linked assay for the rapid quantification of microRNAs based on the viral suppressor of RNA silencing protein p19. *Anal. Biochem. 412*, 165−172.

(14) Lakatos, L., Szittya, G., Silhavy, D., and Burgyan, J. (2004) Molecular mechanism of RNA silencing suppression mediated by p19 protein of tombusviruses. *EMBO J. 23*, 876−884.

(15) Cheng, J., Sagan, S. M., Assem, N., Koukiekolo, R., Goto, N. K., and Pezacki, J. P. (2007) Stabilized recombinant suppressors of RNA silencing: Functional effects of linking monomers of Carnation Italian Ringspot virus p19. *Biochim. Biophys. Acta 1774*, 1528−1535.

(16) Koukiekolo, R., Jakubek, Z. J., Cheng, J., Sagan, S. M., and Pezacki, J. P. (2009) Studies of a viral suppressor of RNA silencing p19-CFP fusion protein: a FRET-based probe for sensing double-stranded fluorophore tagged small RNAs. *Biophys. Chem. 143*, 166−169.

(17) Esquela-Kerscher, A., and Slack, F. J. (2006) Oncomirs - microRNAs with a role in cancer. *Nat. Rev. Cancer 6*, 259−269.

(18) Sarnow, P., Jopling, C. L., Norman, K. L., Schutz, S., and Wehner, K. A. (2006) MicroRNAs: expression, avoidance and subversion by vertebrate viruses. *Nat. Rev. Microbiol. 4*, 651−659.

(19) Chang, J., Nicolas, E., Marks, D., Sander, C., Lerro, A., Buendia, M. A., Xu, C., Mason, W. S., Moloshok, T., Bort, R., Zaret, K. S., and Taylor, J. M. (2004) miR-122, a mammalian liver-specific microRNA, is processed from hcr mRNA and may downregulate the high affinity cationic amino acid transporter CAT-1. *RNA Biol. 1*, 106−113.

(20) Lagos-Quintana, M., Rauhut, R., Yalcin, A., Meyer, J., Lendeckel, W., and Tuschl, T. (2002) Identification of tissue-specific microRNAs from mouse. *Curr. Biol. 12*, 735−739.

(21) Henke, J. I., Goergen, D., Zheng, J., Song, Y., Schuttler, C. G., Fehr, C., Junemann, C., and Niepmann, M. (2008) microRNA-122 stimulates translation of hepatitis C virus RNA. *EMBO J. 27*, 3300−3310.

(22) Jangra, R. K., Yi, M., and Lemon, S. M. (2010) Regulation of hepatitis C virus translation and infectious virus production by the microRNA miR-122. *J. Virol. 84*, 6615−6625.

(23) Jopling, C. L., Schutz, S., and Sarnow, P. (2008) Position-dependent function for a tandem microRNA miR-122-binding site located in the hepatitis C virus RNA genome. *Cell Host Microbe 4*, 77−85.

(24) Jopling, C. L., Yi, M., Lancaster, A. M., Lemon, S. M., and Sarnow, P. (2005) Modulation of hepatitis C virus RNA abundance by a liver-specific MicroRNA. *Science 309*, 1577−1581.

(25) Lanford, R. E., Hildebrandt-Eriksen, E. S., Petri, A., Persson, R., Lindow, M., Munk, M. E., Kauppinen, S., and Orum, H. (2010) Therapeutic silencing of microRNA-122 in primates with chronic hepatitis C virus infection. *Science 327*, 198−201.

(26) Sagan, S. M., Koukiekolo, R., Rodgers, E., Goto, N. K., and Pezacki, J. P. (2007) Inhibition of siRNA binding to a p19 viral suppressor of RNA silencing by cysteine alkylation. *Angew. Chem., Int. Ed. 46*, 2005−2009.

(27) Omarov, R., Sparks, K., Smith, L., Zindovic, J., and Scholthof, H. B. (2006) Biological relevance of a stable biochemical interaction between the tombusvirus-encoded P19 and short interfering RNAs. *J. Virol. 80*, 3000−3008.

(28) Sreerama, N., and Woody, R. W. (2000) Estimation of protein secondary structure from circular dichroism spectra: Comparison of CONTIN, SELCON, and CDSSTR methods with an expanded reference set. *Anal. Biochem. 287*, 252−260.

(29) Chen, C., Ridzon, D. A., Broomer, A. J., Zhou, Z., Lee, D. H., Nguyen, J. T., Barbisin, M., Xu, N. L., Mahuvakar, V. R., Andersen, M. R., Lao, K. Q., Livak, K. J., and Guegler, K. J. (2005) Real-time quantification of microRNAs by stem-loop RT-PCR. *Nucleic Acids Res. 33*, e179.

(30) Livak, K. J., and Schmittgen, T. D. (2001) Analysis of relative gene expression data using real-time quantitative PCR and the 2(-Delta Delta C(T)) Method. *Methods 25*, 402−408.

(31) Bishop, A. C., Shah, K., Liu, Y., Witucki, L., Kung, C., and Shokat, K. M. (1998) Design of allele-specific inhibitors to probe protein kinase signaling. *Curr. Biol. 8*, 257−266.

(32) Liu, Y., Shah, K., Yang, F., Witucki, L., and Shokat, K. M. (1998) Engineering Src family protein kinases with unnatural nucleotide specificity. *Chem. Biol. 5*, 91−101.

(33) Shah, K., Liu, Y., Deirmengian, C., and Shokat, K. M. (1997) Engineering unnatural nucleotide specificity for Rous sarcoma virus tyrosine kinase to uniquely label its direct substrates. *Proc. Natl. Acad. Sci. U.S.A. 94*, 3565−3570.

(34) Kim, C. A., and Berg, J. M. (1993) Thermodynamic beta-sheet propensities measured using a zinc-finger host peptide. *Nature 362*, 267−270.

(35) Minor, D. L. Jr., and Kim, P. S. (1994) Measurement of the beta-sheet-forming propensities of amino acids. *Nature 367*, 660−663.

(36) Minor, D. L. Jr., and Kim, P. S. (1994) Context is a major determinant of beta-sheet propensity. *Nature 371*, 264−267.

(37) Smith, C. K., Withka, J. M., and Regan, L. (1994) A thermodynamic scale for the beta-sheet forming tendencies of the amino acids. *Biochemistry 33*, 5510−5517.

(38) Cheng, J., Koukiekolo, R., Kieliszkiewicz, K., Sagan, S. M., and Pezacki, J. P. (2009) Cysteine residues of Carnation Italian Ringspot virus p19 suppressor of RNA silencing maintain global structural integrity and stability for siRNA binding. *Biochim. Biophys. Acta 1794*, 1197−1203.

(39) Checovich, W. J., Bolger, R. E., and Burke, T. (1995) Fluorescence polarization--a new tool for cell and molecular biology. *Nature 375*, 254−256.

(40) Lundblad, J. R., Laurance, M., and Goodman, R. H. (1996) Fluorescence polarization analysis of protein-DNA and protein-protein interactions. *Mol. Endocrinol. 10*, 607−612.

(41) Vihinen, M. (1987) Relationship of protein flexibility to thermostability. *Protein Eng. 1*, 477−480.

(42) Zavodszky, P., Kardos, J., Svingor., and Petsko, G. A. (1998) Adjustment of conformational flexibility is a key event in the thermal adaptation of proteins. *Proc. Natl. Acad. Sci. U.S.A. 95*, 7406−7411.

(43) Kalodimos, C. G., Biris, N., Bonvin, A. M., Levandoski, M. M., Guennuegues, M., Boelens, R., and Kaptein, R. (2004) Structure and flexibility adaptation in nonspecific and specific protein-DNA complexes. *Science 305*, 386−389.

(44) Macrae, I. J., Li, F., Zhou, K., Cande, W. Z., and Doudna, J. A. (2006) Structure of Dicer and mechanistic implications for RNAi. *Cold Spring Harb. Symp. Quant. Biol. 71*, 73−80.

(45) Ramesh, A., Savva, C. G., Holzenburg, A., and Sacchettini, J. C. (2007) Crystal structure of Rsr, an ortholog of the antigenic Ro protein, links conformational flexibility to RNA binding activity. *J. Biol. Chem. 282*, 14960−14967.

(46) Chu, M., Desvoyes, B., Turina, M., Noad, R., and Scholthof, H. B. (2000) Genetic dissection of tomato bushy stunt virus p19-protein-mediated host-dependent symptom induction and systemic invasion. *Virology 266*, 79−87.

(47) Turina, M., Omarov, R., Murphy, J. F., Bazaldua-Hernandez, C., Desvoyes, B., and Scholthof, H. B. (2003) A newly identified role for Tomato bushy stunt virus P19 in short distance spread. *Mol. Plant Pathol. 4*, 67−72.

(48) Hsieh, Y. C., Omarov, R. T., and Scholthof, H. B. (2009) Diverse and newly recognized effects associated with short interfering RNA binding site modifications on the Tomato bushy stunt virus p19 silencing suppressor. *J. Virol. 83*, 2188−2200.

(49) Lupberger, J., Brino, L., and Baumert, T. F. (2008) RNAi: a powerful tool to unravel hepatitis C virus-host interactions within the infectious life cycle. *J. Hepatol. 48*, 523−525.